ESCUELA DE CONSTRUCCIÓN CIVIL
FACULTAD DE INGENIERÍA
Revista de la Construcción
Journal of Construction

Research Article

Simulation of the behavior of reinforced concrete rectangular hollow sandwich plates under the effect of contact explosion through SPH method

Dursun Bakır [1*], Sedat Savaş [2], Hasan Üstündağ [3]

[1] Department of Civil Engineering, Faculty of Engineering and Architecture, Bitlis Eren University, Bitlis (Türkiye), dbakir@beu.edu.tr
[2] Department of Civil Engineering, Faculty of Engineering, Fırat University, Elazığ (Türkiye), ssavas@firat.edu.tr
[3] Department of Civil Engineering, Faculty of Engineering, Fırat University, Elazığ (Türkiye), hsn.ustundag23@gmail.com
*Correspondence: dbakir@beu.edu.tr (D. Bakir)

Received: 23.01.23; **Accepted:** 14.05.24; **Published:** 12.12.24

Citation: Bakır, D., Savaş, S., Üstündağ., H. (2024). Simulation of the behavior of reinforced concrete rectangular hollow sandwich plates under the effect of contact explosion through SPH method. Revista de la Construcción. Journal of Construction, 23(3), 554-567. https://doi.org/10.7764/RDLC.23.3.554

Highlights:

- During the contact explosion of reinforced concrete hollow slabs, the explosive energy was absorbed by the hollow spaces and released without causing damage to the back surface of the slab.
- The release of blast energy can be achieved by variations in geometric structure without using additional reinforcement methods.
- The investigation revealed that sandwich plates with a consistent hollow height/width had different damage and pressure distributions during contact blast evaluations and that TNT equivalent explosive weight affected crater size.

Abstract: When dealing with contact explosion, a type of explosion load that has a substantial impact on structures, it is necessary to use a distinct approach compared to other types of explosion loads. Hence, utmost significance should be attributed to the selection of the analytical approach when modeling the explosion. It is crucial to ascertain the behavior of the explosion pressure in the space between hollow sandwich plates. This work involved conducting experiments to examine the accurate simulation of hollow plates subjected to contact explosions, which result in a reduction in the dispersion of explosive pressure. The structure was modeled using smooth particle hydrodynamics (SPH) and Lagrangian modeling techniques, taking into account the effects of explosives and contact explosions. The mesh-free structure of these approaches makes them highly successful in resolving significant deformations resulting from explosions. The comparison criteria included the widths of the crater pits on the upper surface of the plate, the behavior of the explosion pressure in the structure cavity, and the impact of the explosion load on the lower section of the plate. After evaluating several explosion load and hollow structure modeling methodologies, it was concluded that the most appropriate approach for reproducing the experimental results involved using Smoothed Particle Hydrodynamics (SPH) to model the explosive and Lagrangian method to model the structure.

Keywords: Explosion load, reinforced hollow sandwich plate (RHSP), contact explosion, smooth particle hydrodynamics (SPH), lagrangian method.

List of abbreviations:

ALE - arbitrary Lagrange-Euler
atm - atmospheric pressure
CFD - computational fluid dynamics method
cm - centimeter
ft - fit
g - gravitational acceleration
Gpa - cigapaskal
gr - gram
HE - high-powered explosive
J - Joule
K - Kelvin
kg - kilogram
KJ - kilojoule
kPa - kilopaskal
lb - libre
lt - litre
m - meter
mm - millimeter
MM-ALE - multi material arbitrary Lagrange-Euler
MPa - megapaskal
ms - milliseconds
N - newton
Pa - Paskal
Psi - bar
RHA - rolled homogeneous armor
s - second
SPH - smooth particle hydrodynamics
TNG - trinitrogliserin

1. Introduction

Various causes can significantly weaken the structural integrity of structures and their components. One example of loads that have a significant influence is the explosion instance. The explosion generates pressure waves that inflict harm upon the structures (Savaş and Bakir, 2023). Extensive research has been conducted in recent years to mitigate this issue. Several studies have reinforced structural elements using different materials (Liao et al., 2022; Nguyen et al., 2021; Tabatabaei et al., 2013; W. Wang et al., 2022), increased the sizes of the elements (Dua and Braimah, 2020; Savaş and Bakir, 2022; C. Zhao et al., 2020), or studied other types of materials (Z. Li et al., 2018; J. Liu et al., 2022; Trajkovski et al., 2017; C. Zhao et al., 2019). In the literature, the investigations focused on the design of hollow plates. These plates were constructed, reinforced, and subjected to both pre- and post-tensioning before being detonated. A study conducted by Azer Maazoun et al. (Maazoun et al., 2019) focused on reinforcing the upper sections of hollow sandwich plates using carbon fiber and conducting near-explosion trials. One plate served as a reference sample, while the remaining plates were strengthened with varying quantities of carbon fiber. An explosive device of the C4 variety was positioned at a stand-off distance of 0.5 meters in the central apertures and lower sections of the samples.

The weight of the explosive utilized in the experiments was 1.5 kg. The sandwich plates in the study had a length of 6 meters and a width of 0.6 meters. The sandwich plates with hollow interiors were simulated and examined in Ansys Ls-Dyna

software utilizing the Lagrange Method. The analysis demonstrated that the resistance of the hollow sandwich plates, which were reinforced with carbon fiber, was enhanced against explosion. Furthermore, the numerical analysis yielded results that were consistent with the experimental findings. In the investigation conducted by Yılmazer Polat et al. (2023), the researchers created plates of different thicknesses using C50 reinforced concrete. The plates were created using layers of steel plates and had dimensions of 150×150 cm. Plates composed of steel fiber, rock wool, and ceramic wool fibers, each with different reinforcing ratios, underwent testing to assess their ability to withstand contact explosions. The Rpg-7 impact test was conducted using a TNT equivalent explosive. The greater resistance to explosives was attributed to the material's compact and dense composition, rather than relying on a high reinforcement ratio in the concrete. Although the structure was penetrated, there was no alteration in the static.

The use of steel fiber in the concrete did not result in a significant effect. The spaced plate effectively mitigated the impact of RPG-7 missiles by absorbing 50% of their energy. In the study conducted by Castedo et al. (Castedo et al., 2021), near-explosion experiments were carried out using 3 reinforced concrete plates made of C25-type concrete. The stand-off distances in the explosion experiments were changed to 0.5 m and 1 m. Three different explosive geometries were selected in the study. The slabs were analyzed using coupled FEM-SPH. In addition, it is stated that the SPH method used in the numerical modeling of explosives increases the accuracy of the analysis and that if the FEM method is used in a phenomenon that creates high deformations such as an explosion, the explosion does not spread along the slab surface as in reality. In the study conducted by Zhao et al. (X. Zhao et al., 2018), a contact explosion experiment was performed using 1 kg of TNT explosives on reinforced concrete plates of size (1 x 2 x 0.1) m reinforced with wire mesh. In the study, numerical models of reinforced concrete plates were created and numerical analysis was performed in Ansys Autodyn software by using coupled Lagrange-Euler, coupled Lagrange-SPH, and only SPH methods.

The analysis time was set as 6 ms in the program. As a result of the study, the explosive gave results closer to reality when modeled with the SPH method. In addition, it is stated that the most compatible analysis method for experimental studies is coupled Lagrange-SPH. In the study conducted by Jun Li et al. (J. Li et al., 2017), contact explosion experiments were performed on reinforced concrete plates with 10, 20 and 30 layers of a wire mesh made of 60 MPa concrete with a size of 2 x 0.8 x 0.12 m. In the study, TNT explosive weighing 1 kg was used and numerical analysis was performed in Ls-Dyna software by choosing coupled FEM-SPH method. The plate concrete was modeled as solid and the reinforcements were modeled as beam elements. The explosive in the analyses was modeled using the SPH method. As a result of the study, the crater pit in the samples with wire mesh shrank and the analyzes overlapped with the experiments at a reasonable level. In the study conducted by Karmakar et al. (2021), explosion analysis was performed using TNT explosives on reinforced concrete plates with a size of 4 x 4 x 0.3 m. Lagrange, MM-ALE, and coupled Lagrange/MM-ALE methods were used in the analyses. In the analysis made by the Lagrange method, explosives and air were not modeled, the explosion pressure was calculated experimentally and applied on the slab. In the MM-ALE method, the slab was modeled by the Lagrange, as well as, explosive and air were modeled by the Euler method. In this method, it is stated that the explosive weight, explosion speed, and explosive diameter are important. In addition to these three methods used in the study, the coupled FEM-SPH model was also created for the analyses.

The reason for this is stated as serious mesh distortions and errors in the analysis will occur if finite element-based methods are used completely in the explosion. In this model, the slab was analyzed with FEM and the explosive was analyzed with SPH. The fluid flow model is taken into account for the calculation of explosive particles (SPH particles). In other words, the problem was transformed into a kind of fluid-structure interaction problem. We determined that the most successful method in the study was coupled FEM-SPH. When the explosion event is examined, SPH is seen as the most appropriate method in terms of the spread of the explosion wave formed by the detonation of the explosive and the maximum pressure formed on the surface (Castedo et al., 2018; Fan and Li, 2017; M. B. Liu et al., 2017; J. Wang et al., 2020).

When the studies in the literature were examined, it was seen that plate design and reinforcement applications were made to increase the explosion resistance of the samples in contact and near-contact experiments. In the explosion experiments performed on the plates designed as hollow-core, the plates were pre-tensioned (Kakogiannis et al., 2013; Kodur and Shakya, 2017; Maazoun et al., 2017, 2019). However, in the previous studies in the literature, contact explosion experiments have not

been performed on reinforced hollow-core samples. We determined that the use of only finite element-based methods (Euler, Lagrange, ALE, MM-ALE, etc.) in explosion analysis will cause serious mesh distortions and deviations in the analysis of explosion that causes high deformation.

In this study, concrete with a compressive strength of 35N/mm² was reinforced with Q131/131 wire mesh with a diameter of 6 mm and rectangular hollow plates of different sizes were manufactured. A comparison was made with numerical modeling techniques of contact explosion experiments on reinforced concrete hollow sandwich plates (RHSP) using explosives of different TNT equivalent weights, and a model was determined to simulate the real behavior of hollow plates under the influence of contact explosion. Taking into account previous studies in the literature and the fact that high deformation will occur as a result of contact explosion, we determined that the most suitable method for this type of experiment is coupled FEM-SPH.

2. Materials and methods

2.1. *Hollow sandwich plates preparation*

The RHSP samples used in contact explosion investigations are composed of reinforced concrete (RC) hollow sandwich plates, which consist of a top plate, inner plate, and bottom plate. The plates are labeled as H-B, where H represents the height of the gap, and B represents the breadth of the hollow (see Figure 1). The RHSPs in the study have a top plate and bottom plate thickness of 50 mm. These plates are strengthened with wire mesh that includes 6 mm diameter reinforcements. Furthermore, 13 pieces of 6 mm reinforcements were positioned on the inner plate surface, creating a hollow space of 150 mm. The specimens were fabricated utilizing concrete having a compressive strength of 35 N/mm² (Table 1). All slabs were constructed using the identical concrete mixture Table 2) and reinforcement bars (Table 3). Given that the explosion experiments include placing the plates on the ground, the modeling ensures that the bottom of the plates is adequately supported.

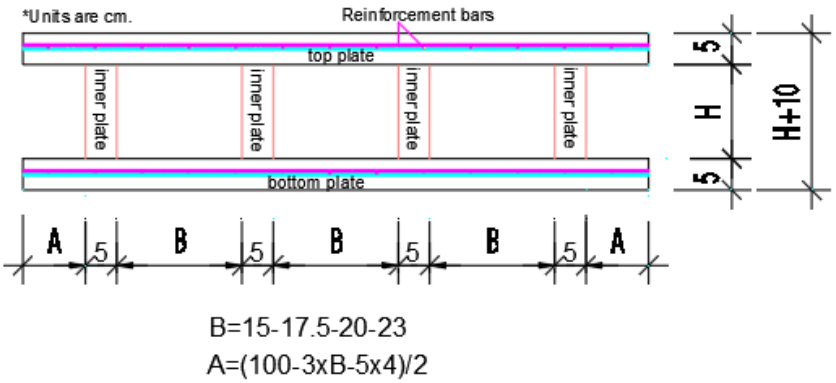

Figure 1. Cross-section of RHSP samples.

Table 1. RHSP types.

Sample No.	Type	H/B (mm)	Concrete class	Reinforcement
1	H15-15	150/150	C35	Q131/131
2	H15-17,5	150/175	C35	Q131/131
3	H15-20	150/200	C35	Q131/131
4	H17,5-15	175/150	C35	Q131/131
5	H17,5-23	175/230	C35	Q131/131
6	H20-15	200/150	C35	Q131/131
7	H20-20	200/200	C35	Q131/131
8	H20-23	200/230	C35	Q131/131
9	H20-26	200/260	C35	Q131/131

Table 2. Concrete mixing ratios.

Cement	16%
Aggregate (7-14 mm diameter)	35.40%
Aggregate (3-9 mm diameter)	4.40%
Sand	37.60%
Water	6.40%
Additive	0.20%

Table 3. Q131/131 steel wire mesh.

Reinforcement range	150 m
Reinforcement diameter	5.0 mm
Reinforcement cross-sectional area	1.31 m²
Bidirectional reinforcement rate	0.35%

2.2. *Contact explosion experiments*

The experimental setup shown in Figure 2 was prepared for the RHSPs used in the study. In contact explosion experiments, the explosive with a TNT equivalence of 0.62 (McVay, 1988; Zhou et al., 2008) was put in cube-shaped molds and placed on the top surface of the plate. TNT equivalent explosive quantities in contact explosion tests for RHSP samples are given in Table 4.

Figure 2. Test setup for RHSP samples.

Table 4. Explosive weights used in RHSP samples.

Sample No.	Type	H/B (mm)	TNT-equivalent explosive weight (gr)	Crater pit dimensions width/length (mm)
1	H15-15	150/150	625	150/350
2	H15-17,5	150/175	682	180/340
3	H15-20	150/200	774	210/310
4	H17,5-15	175/150	677	160/290
5	H17,5-23	175/230	937	225/350
6	H20-15	200/150	714	160/310
7	H20-20	200/200	893	200/400
8	H20-23	200/230	1389	400/450
9	H20-26	200/260	1190	250/450

3. Experimental results and analysis

In the literature, Euler, Lagrange, Ale, MMale, and SPH methods have been used in explosion modeling. In these models, various applications have been made by researchers to determine the behavior of the structure against explosion. The techniques with and without mesh have been applied to determine the structural behavior under this loading effect.

3.1. *Euler method*

The Euler approach is based on the fixed finite element mesh model. Numerical methods based on the Euler approach, such as the finite element method, the finite difference method, and the finite volumes method, are used to solve many important problems. However, this method requires re-meshing algorithms for large deformation problems, which increases the cost of calculation. If problems that may cause large deformations (e.g. explosion analysis) are analyzed by the Euler Method, instability occurs in the analysis due to large deterioration in the mesh structure. In addition, studies indicate(Allah, 2012; Karmakar and Shaw, 2021) that determining the precise position of free surfaces, deformable boundaries and moving interfaces in the Euler Method is a challenging task. Figure 3 illustrates the trouble of accurately identifying the locations of the distorted borders of the reference frame and the moving interfaces. The Euler approach distorts the calculation frame in this case.

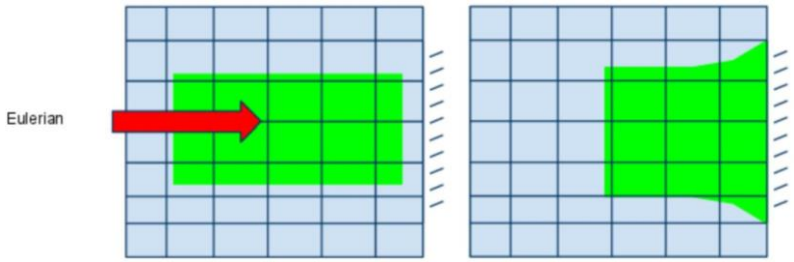

Figure 3. Calculation framework and system behavior in problems analyzed by Euler's Method (Ansys, 2020).

3.2. Lagrange method

In the Lagrange method, the system is represented by separate particles without a constant link. For this reason, the Lagrange method is often used in problems such as explosion, breakage, disintegration, fluid movement, etc. The Lagrange approach is based on the bonding of finite element mesh nodes to the material and their deformation together with the material. While the aforementioned mesh allows easy monitoring of free surfaces and interfaces between different materials, it cannot follow the serious deformation of the computational mesh and can make the algorithm unstable. Under large deformations, the Lagrange approach may not give accurate results due to the deterioration of the mesh structure of the elements and the emergence of modeling inadequacy. To avoid this problem, a thinner mesh procedure is required, which leads to an increase in the analysis time. However, increasing the analysis time also increases the cost of the calculation and is usually not preferred. The "erosion criterion" is needed to analyze large deformations in the elements by the Lagrange method. When this user-defined criterion is reached, the elements begin to wear out.

As noted in the studies (Allah, 2012; Karmakar and Shaw, 2021), this method does not ensure that the analyzed system is preserved as a whole, lacks a physical background, and can lead to the early deletion of elements during analysis. Figure 4 demonstrates that the Lagrange method has resulted in the disappearance of elements during the study. When dealing with solutions that involve significant deformations, the removal of parts poses a challenge to the accuracy of the solution.

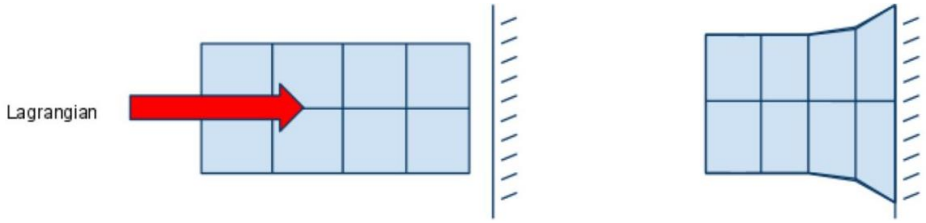

Figure 4. Demonstration of the reference surface and system behavior in problems using the Lagrange method (Ansys, 2020).

The numerical difficulties of the mesh and element-based methods mentioned above restrict their use in problems involving very large deformations. The formation and spread of a large number of cracks, the interaction of cracks, and the deformations encountered when a structure is subjected to explosion loading lead to partial or complete damage to the system. In a study (Karmakar and Shaw, 2021), it was stated that mesh-free methods as an alternative to the Euler and Lagrange methods were more effective in dealing with extreme deformation problems such as an explosion.

3.3. SPH (smooth particle hydrodynamics) method

The SPH Method is a mesh-free Lagrange particle method used to model impact, explosion, or fluid-structure interaction problems (Chen and Lien, 2018; G. R. Liu and Liu, 2003; Z. L. Zhang and Liu, 2019).It has been developed to avoid mesh deterioration encountered in extreme deformations with FEM and to model complex free surface and material interface behaviors. The main difference between the classical methods and the SPH method is that a mesh structure is not defined. The SPH method has been extensively applied to problems involving incompressibility. This method contains particles to process and analyze high deformations with a moving boundary. Particles can move freely according to internal particle interactions or external forces. The word "particle" refers to a region in space. Because field variables are related to these particles, they are found by flattening at any point in space. The SPH method is based on an interpolation technique that obtains the value of a function at any point using values at neighboring points (Du et al., 2016; Hosseini et al., 2007; Lucy, 1977). In SPH, a field function f(x) in the problem area can be written as;

$$\langle f(x)\rangle = \int_{\Omega} f(x')W(x-x',h)\,dx' \qquad (1)$$

The Ω value in equation 1 is the problem area, and f is a field function related to the three-dimensional position vector x. $W(x-x',h)$is a function of the flattening kernel. "h" is the flattening length that defines the area of the flattening kernel function. The flattening kernel function must be chosen to satisfy certain conditions, the first of which is the normalization condition in Equation 2.

$$\int_{\Omega} W(x-x',h)dx' = 1 \qquad (2)$$

The second condition is the property of the Dirac Delta function given in Equation 3:

$$\lim_{h\to 0} W(x-x',h) = \delta(x-x') \qquad (3)$$

The last condition is the compactness property in Equation 4:

$$[\,W(x-x',h),\quad |\,x-x'\,| > (\mathrm{k}\ \mathrm{x}\ h)] \qquad (4)$$

The value k given above represents a scalar factor related to flattening at point x. This value defines the area of the flattening function. This area is called the backing field at point x. According to the multiplication rule and Gauss's Law, the derivative of this function can be written as follows:

$$\langle \nabla . f(x) \rangle = \int_S f(x')\, W(x - x', h). \vec{n} dS - \int_\Omega f(x). \nabla W(x - x', h) dx' \quad (5)$$

The n $\vec{}$ in Equation 5 is the unit vector perpendicular to the surface S. If the backing field is within the problem area, the following can be achieved according to the compactness of the kernel function;

$$[W(x - x', h) = 0] \quad (6)$$
$$[f(x')W(x - x', h) = 0] \quad (7)$$

If the derivatives are arranged according to the conditions in Equation 6 and Equation 7, they can be written as follows:

$$\langle \nabla . f(x) \rangle = -\int_\Omega f(x). \nabla W(x - x', h) dx' \quad (8)$$

A summation is then performed on all the particles within the backing field as shown in Equation 9 and Equation 10:

$$\langle f(x_i) \rangle = \sum_{j=1}^{N} \frac{m_j}{\rho_j} f(x_j) W_{ij} \quad (9)$$
$$\langle \nabla . f(x_i) \rangle = -\sum_{j=1}^{N} \frac{m_j}{\rho_j} f(x_j). \nabla W_{ij} \quad (10)$$

W_{ij} in Equation 10 is calculated as follows;

$$W_{ij} = W(x_i - x_j, h) \quad (11)$$

Figure 5 shows the backing field defined for any "i" particle.

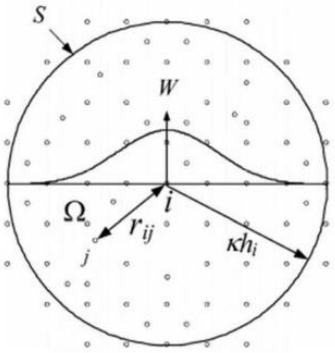

Figure 5. The backing field of particle "i"

The above formulations can be combined with different formulas and rewritten depending on the type of problem being dealt with. Looking at the studies (Gharehdash et al., 2020; Hosseini et al., 2007; G. Wang et al., 2015; A. man Zhang et al., 2017) in the literature, it is seen that the Navier-Stokes equation or Gradient approaches are applied together with the kernel function.

4. Conclusions and comments

Contact explosion experiments were performed on RHSP samples according to their TNT equivalent explosive weights in Table 2, where it was observed that crater pits formed on the upper surface of the RHSPs and that these crater pit sizes varied depending on the explosive weight. However, we observed that deformations occurred in the wire mesh and in the hollows on the upper surface of the RHSPs, but these deformations did not affect the lower surface of the plates. This is because after

the explosion wave passed through the upper surface of the plate, it was evacuated through the hollow and moved towards the lower surface of the plate.

In the numerical analysis of RHSP samples using coupled FEM-SPH method, the explosion time was selected as 1 ms and the analysis time as 3 ms in ANSYS/Autodyn software. In addition, the mesh size was chosen as 19 mm for all RHSP samples, and the element size was chosen as 5 mm for explosives modeled with SPH. Fig.6 shows the distribution of explosive particles (SPH particles) in the analysis. As a result of the analysis, damage and pressure distributions in RHSP samples and the dimensions of the formed crater pit were examined. Of these samples, the sample with the least damage and pressure distribution is H15-15 and the sample with the most damage is H20-23 (Fig.7-8). The findings of the numerical analysis of RHSP samples are shown in Table 5.

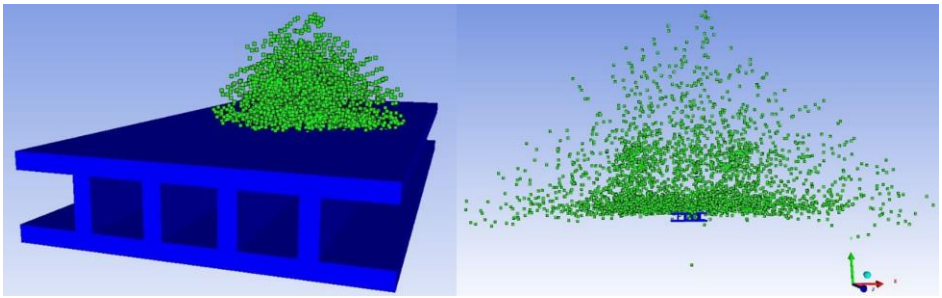

Figure 6. Distribution of explosive particles (SPH particles)

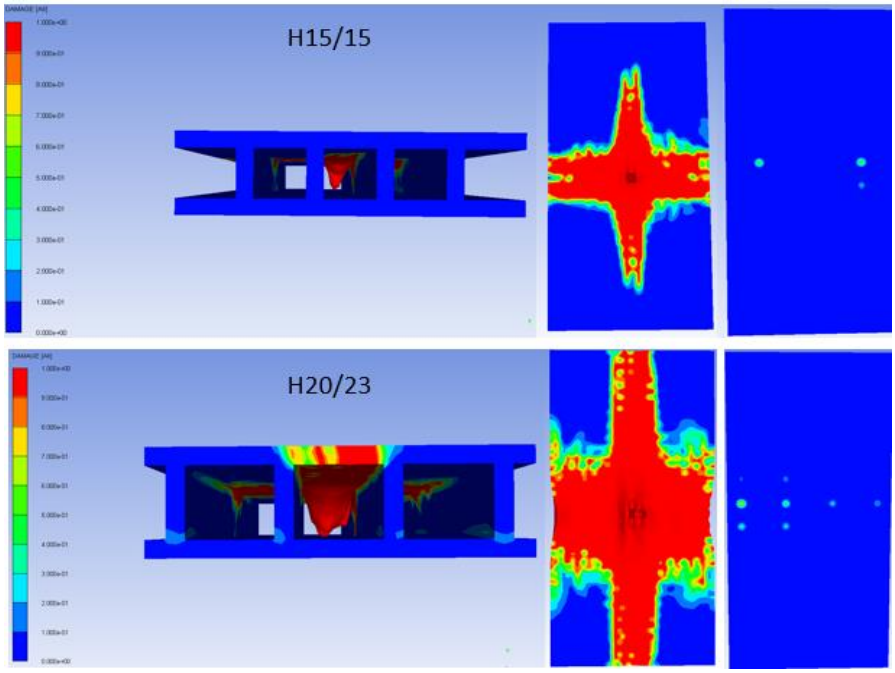

Figure 7. Pressure distribution of H15/15 and H20/23 samples

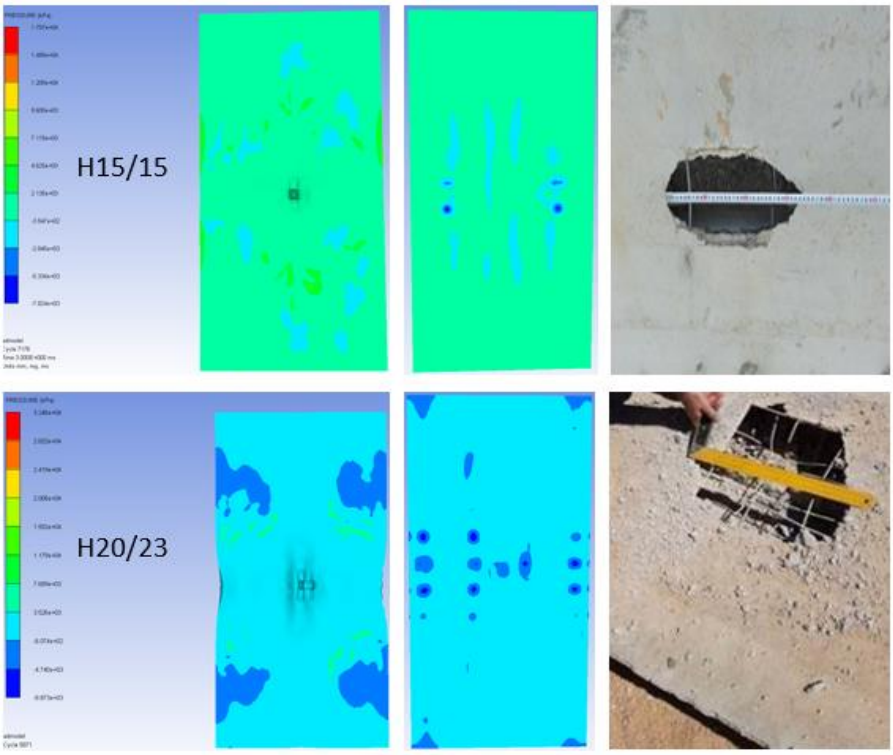

Figure 8. Damage distribution of H15/15 and H20/23 samples

When the coupled FEM-Lagrange was selected, the distribution of the explosive particles occurred as seen in Fig.9. With the selection of element sizes of 5mm and mesh size of 19mm, an explosion time of 1sec and analysis time of 3ms were achieved. However, in this model, the distribution did not occur as in the SPH model and, this model was not experimentally compatible.

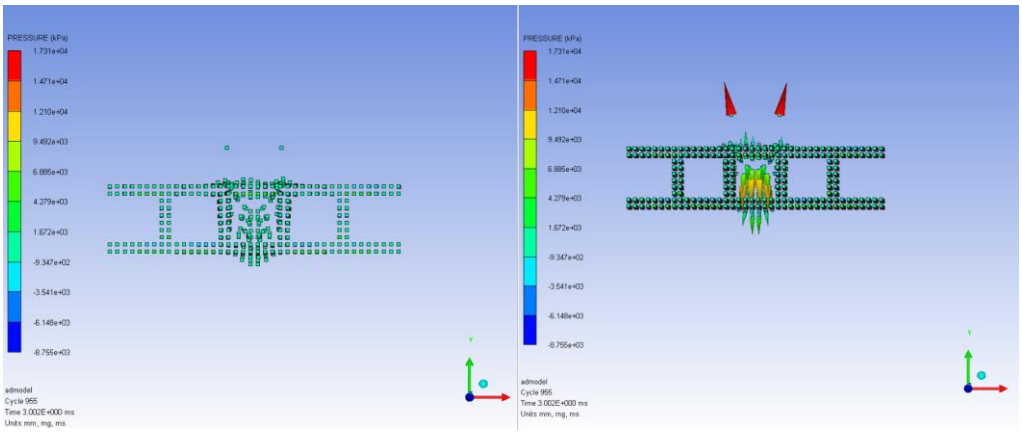

Figure 9. It shows the plate appearance in which the Lagrange is selected for the explosion

In contact explosion tests for samples 2 and 3, the explosive weight increased, but the lowest positive pressure occurred in sample 3 (H15-20) (Table 5). Similarly, the same situation was observed in samples 1 and 3. The damage to the upper surface of sample 9 was greater than that of sample 7. The damage transmitted to the bottom surface was greater in sample 9 than in sample 7. When the pressures in RHSPs 7 and 9 were examined, we found that the positive pressure in sample 9 and the amount of pressure transmitted to the bottom surface were higher. The hollow width of the RHSPs numbered 1, 4, and 6 (H15-15, H17,5-15, and H20-15) is constant (Table 1). As a result of the analysis, we determined that the crater pit in these samples

had rectangular geometry (Table 5). In sample 4, the damage caused by the explosion was found to spread more across the plate surface than in sample 1. However, of the mentioned 3 samples, the sample with the most damage to the upper surface is sample 6 (H20-15). However, the distribution of damage on the lower surfaces of RHSPs No. 1 and No. 4 is similar. In addition, sample 6 made the least damage distribution on the bottom surface. When samples 1 and 4 were examined, it was found that the amount of TNT equivalent explosive used in the experiments increased in sample 4, but the maximum positive pressure obtained in the analysis for this sample decreased compared to sample 1.

Although 714 g TNT equivalent explosive was used in sample 6, the maximum amount of positive pressure obtained in numerical analysis for sample 6 was lower than in sample 1. The pressure distribution on the upper surface of sample 4 was higher than that of sample 1. However, in both samples, the pressures on the bottom surface spread throughout the hollow and were also collected at some points close to where the explosive was placed. The explosion pressure spread more on the upper and lower surfaces of sample 6 compared to samples 1 and 4. The hollow widths of samples 5 and 8 (H17,5-23 and H20-23) are constant (Table 1). In sample 8, more TNT equivalent explosives were used than in sample 5 (Table 4). The crater pits obtained in the experiments for samples 8 and 5 have a "rectangular" geometry, but as the number of explosives increased, this geometry approached the "square" (Table 5).

The distribution of damage on the upper and lower surfaces of sample 8 was more than that of sample 5. The maximum positive pressure obtained as a result of the numerical analysis of sample 8 was higher than that of sample 5, but the minimum negative pressure obtained as a result of the numerical analysis of sample 5 was more than sample 8 (Table 5). The pressure distribution on the upper surface of sample 5 showed a wider distribution than sample 8. Also, the pressure on the lower surface of sample 5 was distributed throughout the hollow, while the explosion pressure was gathered at certain points in sample 8.

Table 5. Experimental results and analysis results of crater dimensions

Sample No.	Type	The width/height dimensions of the crater pit in the experiment (mm)	The width/height dimensions of the crater pit in the analysis (mm)	The margin of error for the width/height of the crater pit (%)	Maximum positive pressure in the analysis (KPa)	Minimum negative pressure in the analysis (KPa)
1	H15-15	150/350	150/350	0/0	$1{,}707x10^4$	$-7{,}824x10^3$
2	H15-17,5	180/340	170/340	5,56/0	$2{,}184x10^4$	$-7{,}904x10^3$
3	H15-20	210/310	200/300	4,76/3,23	$1{,}311x10^4$	$-8{,}361x10^3$
4	H17,5-15	160/290	200/280	25/3,45	$1{,}075x10^4$	$-7{,}728x10^3$
5	H17,5-23	225/350	200/400	11,11/14,28	$2{,}259x10^4$	$-9x10^3$
6	H20-15	160/310	150/300	6,25/3,23	$1{,}242x10^4$	$-7{,}926x10^3$
7	H20-20	200/400	180/360	10/10	$1{,}441x10^4$	$-8{,}268x10^3$
8	H20-23	400/450	300/550	25/22,22	$3{,}246x10^4$	$-8{,}873x10^3$
9	H20-26	250/450	250/500	0/11,11	$3{,}311x10^4$	$-8{,}540x10^3$

The simulation involved utilizing meshed and free mesh modeling tools to analyze the response of hollow sandwich plates to contact explosion. The simulations were used to identify the strategies that most accurately mirrored the experimental data. The coupled finite element method (FEM) and smoothed particle hydrodynamics (SPH) method, known for its effectiveness in numerical study of explosions, was chosen for the contact explosion analysis. A comparison was made between the results obtained from numerical analyses and experimentation. Furthermore, the study also investigated the impact of RHSP cross-sectional geometries on explosion resistance. Conclusively, the study revealed that the damage distributions following the

explosion escalated in proportion to the amount of explosive weight applied to the upper surface of the RHSP samples. As a result, the size of the crater pit on the RHSP upper surfaces likewise grew larger.

As the dimensions of the hollow space (height x width) in the RHSPs increased, the pressure wave resulting from the contact explosion was distributed along the hollow direction and expelled from the space between the inner webs. Numerical analyses revealed that this led to reduced damage to the subsurfaces of the RHSP.

The numerical analysis model is compatible with experimental studies because it allows for the analysis of mesh distortions and pressure distributions that occur during explosion events with high deformations. This analysis is done using solution techniques such as the Lagrange method for the plate model and the SPH method for explosives. Upon analyzing the error margins of crater pits that formed in RHSPs following the explosion (as shown in Table 5), we saw that the results obtained from the SPH analysis in Autodyn were in agreement with the experimental findings.

- Upon examination of the Coupled FEM-Lagrange model, it was determined that the explosive used in the experiment was not suitable for the particle distribution and damage behavior of the plates.

Author contributions: Bakır and Savas: conceptualization, methodology, formal analysis, writing –reviewand editing, supervision.Ustundag: visualization, writing –reviewand editing, formal analysis.

Funding: not applicable.

Acknowledgments: This study was carried out with the support of the TÜBİTAK 1001 Project, numbered 219M392.

Conflicts of interest: the authors declare that they have no conflict of interest

References

Allah, A. M. A. A. (2012). An Improved Incompressible Smoothed Particle Hydrodynamics to Simulate Fluid-Soil-Structure Interactions.

Ansys. (2020). ANSYS Explicit Dynamics Analysis Guide. January, 394.

Castedo, R., Natale, M., López, L. M., Sanchidrián, J. A., Santos, A. P., Navarro, J., and Segarra, P. (2018). Estimation of Jones-Wilkins-Lee parameters of emulsion explosives using cylinder tests and their numerical validation. International Journal of Rock Mechanics and Mining Sciences, 112, 290–301. https://doi.org/10.1016/j.ijrmms.2018.10.027

Castedo, R., Santos, A. P., Alañón, A., Reifarth, C., Chiquito, M., López, L. M., Martínez-Almajano, S., and Pérez-Caldentey, A. (2021). Numerical study and experimental tests on full-scale RC slabs under close-in explosions. Engineering Structures, 231(August 2020). https://doi.org/10.1016/j.engstruct.2020.111774

Chen, J. Y., and Lien, F. S. (2018). Simulations for soil explosion and its effects on structures using SPH method. International Journal of Impact Engineering, 112(October 2017), 41–51. https://doi.org/10.1016/j.ijimpeng.2017.10.008

Du, Y., Ma, L., Zheng, J., Zhang, F., and Zhang, A. (2016). Coupled simulation of explosion-driven fracture of cylindrical shell using SPH-FEM method. International Journal of Pressure Vessels and Piping, 139–140, 28–35. https://doi.org/10.1016/j.ijpvp.2016.03.001

Dua, A., and Braimah, A. (2020). Assessment of Reinforced Concrete Slab Response to Contact Explosion Effects. Journal of Performance of Constructed Facilities, 34(4). https://doi.org/10.1061/(asce)cf.1943-5509.0001469

Fan, H., and Li, S. (2017). A Peridynamics-SPH modeling and simulation of blast fragmentation of soil under buried explosive loads. Computer Methods in Applied Mechanics and Engineering, 318, 349–381. https://doi.org/10.1016/j.cma.2017.01.026

Gharehdash, S., Barzegar, M., Palymskiy, I. B., and Fomin, P. A. (2020). Blast induced fracture modelling using smoothed particle hydrodynamics. International Journal of Impact Engineering, 135(January 2019), 103235. https://doi.org/10.1016/j.ijimpeng.2019.02.001

Hosseini, S. M., Manzari, M. T., and Hannani, S. K. (2007). A fully explicit three-step SPH algorithm for simulation of non-Newtonian fluid flow. International Journal of Numerical Methods for Heat and Fluid Flow, 17(7), 715–735. https://doi.org/10.1108/09615530710777976

Kakogiannis, D., Pascualena, F., Reymen, B., Pyl, L., Ndambi, J. M., Segers, E., Lecompte, D., Vantomme, J., and Krauthammer, T. (2013). Blast performance of reinforced concrete hollow core slabs in combination with fire: Numerical and experimental assessment. Fire Safety Journal, 57, 69–82. https://doi.org/10.1016/j.firesaf.2012.10.027

Karmakar, S., and Shaw, A. (2021). Response of R.C. plates under blast loading using FEM-SPH coupled method. Engineering Failure Analysis, 125(April), 105409. https://doi.org/10.1016/j.engfailanal.2021.105409

Kodur, V. K. R., and Shakya, A. M. (2017). Factors governing the shear response of prestressed concrete hollowcore slabs under fire conditions. Fire Safety Journal, 88(October 2015), 67–88. https://doi.org/10.1016/j.firesaf.2017.01.003

Li, J., Wu, C., Hao, H., and Su, Y. (2017). Experimental and numerical study on steel wire mesh reinforced concrete slab under contact explosion. Materials and Design, 116, 77–91. https://doi.org/10.1016/j.matdes.2016.11.098

Li, Z., Liu, Y., Yan, J. bo, Yu, W. li, and Huang, F. lei. (2018). Experimental investigation of p-section concrete beams under contact explosion and close-in explosion conditions. Defence Technology, 14(5), 540–549. https://doi.org/10.1016/j.dt.2018.07.025

Liao, Q., Yu, J., Xie, X., Ye, J., and Jiang, F. (2022). Experimental study of reinforced UHDC-UHPC panels under close-in blast loading. Journal of Building Engineering, 46(January 2021), 103498. https://doi.org/10.1016/j.jobe.2021.103498

Liu, G. R., and Liu, M. B. (2003). Smoothed Particle Hydrodynamics. In World scientific (Vol. 4, Issue 1). WORLD SCIENTIFIC. https://doi.org/10.1142/5340

Liu, J., Hu, H., Li, J., Chen, Y. F., and Zhang, L. (2022). Flexural behavior of assembled monolithic long-span composite beams with CIP reinforced concrete layer atop precast hollow core slabs. Journal of Building Engineering, 46(August 2021), 103791. https://doi.org/10.1016/j.jobe.2021.103791

Liu, M. B., Zhang, Z. L., and Feng, D. L. (2017). A density-adaptive SPH method with kernel gradient correction for modeling explosive welding. Computational Mechanics, 60(3), 513–529. https://doi.org/10.1007/s00466-017-1420-5

Lucy, L. B. (1977). A numerical approach to the testing of the fission hypothesis. The Astronomical Journal, 82, 1013. https://doi.org/10.1086/112164

Maazoun, A., Matthys, S., Belkassem, B., Lecompte, D., and Vantomme, J. (2019). Blast response of retrofitted reinforced concrete hollow core slabs under a close distance explosion. Engineering Structures, 191(May), 447–459. https://doi.org/10.1016/j.engstruct.2019.04.068

Maazoun, A., Matthys, S., Vantomme, J., Belkassem, B., and Mourão, R. (2017). Numerical Prediction of the Dynamic Response of Reinforced Concrete Hollow Core Slabs under Blast Loading. 10th European LS-Dyna Conference, Salzburg, Austria 2017, fig 2, 1–8.

McVay, M. K. (1988). Spall Damage of Concrete Structures (Final Report). Technical Report SL-88-22, Technical Report, 431.

Nguyen, H. T. N., Li, Y., and Tan, K. H. (2021). Shear behavior of fiber-reinforced concrete hollow-core slabs under elevated temperatures. Construction and Building Materials, 275. https://doi.org/10.1016/j.conbuildmat.2020.121362

Polat, B. Y., Savaş, S., and Polat, A. (2023). Anti-tank impact absorption with a reinforced concrete plate design. Advances in Concrete Construction, 15(4), 229–239. https://doi.org/10.12989/acc.2023.15.4.229

Savaş, S., and Bakir, D. (2022). An experimental study on the blast responses of hollow core concrete slabs to contact explosions. Revista de La Construcción, 21(3), 587–601. https://doi.org/10.7764/RDLC.21.3.587

Savaş, S., and Bakir, D. (2023). An investigation of the effects of the vehicle terror suicide attack in the urban area. Engineering Failure Analysis, 145, 107049. https://doi.org/10.1016/j.engfailanal.2023.107049

Tabatabaei, Z. S., Volz, J. S., Baird, J., Gliha, B. P., and Keener, D. I. (2013). Experimental and numerical analyses of long carbon fiber reinforced concrete panels exposed to blast loading. International Journal of Impact Engineering, 57, 70–80. https://doi.org/10.1016/j.ijimpeng.2013.01.006

Trajkovski, J., Kunc, R., and Prebil, I. (2017). Blast response of centrally and eccentrically loaded flat-, U-, and V-shaped armored plates: comparative study. Shock Waves, 27(4), 583–591. https://doi.org/10.1007/s00193-016-0704-6

Wang, G., Liu, G., Peng, Q., De, S., Feng, D., and Liu, M. (2015). A 3D smoothed particle hydrodynamics method with reactive flow model for the simulation of ANFO. Propellants, Explosives, Pyrotechnics, 40(4), 566–575. https://doi.org/10.1002/prep.201400244

Wang, J., Zhang, Y., Qin, Z., Song, S., and Lin, P. (2020). Analysis method of water inrush for tunnels with damaged water-resisting rock mass based on finite element method-smooth particle hydrodynamics coupling. Computers and Geotechnics, 126(June), 103725. https://doi.org/10.1016/j.compgeo.2020.103725

Wang, W., Huo, Q., Yang, J. chao, Wang, J. hui, and Wang, X. (2022). Experimental investigation of ultra-early-strength cement-based self-compacting high strength concrete slabs (URCS) under contact explosions. Defence Technology, xxxx. https://doi.org/10.1016/j.dt.2022.02.010

Zhang, A. man, Sun, P. nan, Ming, F. ren, and Colagrossi, A. (2017). Smoothed particle hydrodynamics and its applications in fluid-structure interactions. Journal of Hydrodynamics, 29(2), 187–216. https://doi.org/10.1016/S1001-6058(16)60730-8

Zhang, Z. L., and Liu, M. B. (2019). Numerical studies on explosive welding with ANFO by using a density adaptive SPH method. Journal of Manufacturing Processes, 41(March), 208–220. https://doi.org/10.1016/j.jmapro.2019.03.039

Zhao, C., Lu, X., Wang, Q., Gautam, A., Wang, J., and Mo, Y. L. (2019). Experimental and numerical investigation of steel-concrete (SC) slabs under contact blast loading. Engineering Structures, 196(April). https://doi.org/10.1016/j.engstruct.2019.109337

Zhao, C., Ye, X., He, K., and Gautam, A. (2020). Numerical study and theoretical analysis on blast resistance of fabricated concrete slab. Journal of Building Engineering, 32(August), 101760. https://doi.org/10.1016/j.jobe.2020.101760

Zhao, X., Wang, G., Lu, W., Yan, P., Chen, M., and Zhou, C. (2018). Damage features of RC slabs subjected to air and underwater contact explosions. Ocean Engineering, 147(November 2017), 531–545. https://doi.org/10.1016/j.oceaneng.2017.11.007

Zhou, X. Q., Kuznetsov, V. A., Hao, H., and Waschl, J. (2008). Numerical prediction of concrete slab response to blast loading. International Journal of Impact Engineering, 35(10), 1186–1200. https://doi.org/10.1016/j.ijimpeng.2008.01.004